

# Combining DFT with ML to study size specific interactions between metal clusters and adsorbates

Shweta Mehta,<sup>†,‡</sup> Sheena Agarwal,<sup>†,‡</sup> and Kavita Joshi<sup>\*,†,‡</sup>

<sup>†</sup> *Physical and Materials Chemistry Division, CSIR-National Chemical Laboratory, Dr.*

*Homi Bhabha Road, Pashan, Pune-411008, India.*

<sup>‡</sup> *Academy of Scientific and Innovative Research (AcSIR)*

E-mail: k.joshi@ncl.res.in;kavita.p.joshi@gmail.com

## Abstract

To date, density functional theory (DFT) is one of the most accurate and yet practical theory to gain insight about materials properties. Although successful, the computational cost is the main hurdle even today. A way out is combining DFT with machine learning (ML) to reduce the computational cost without compromising accuracy. However, the success of this approach hinges on the correctness of the descriptors. In the present work, we demonstrate that, based on *only* interatomic distances as descriptors, our ML model predicts interaction energy between an adsorbate and Al cluster with absolute mean error (AME)  $\sim 0.05$  eV (or less) and reproduces the PES experienced by an incoming atom. Our extensive DFT calculations reveal that atoms experiencing identical environment within a cluster have identical interaction energy patterns. Further, we demonstrate that our model is not specific to Al clusters, and could be applied to clusters of different elements as well. Its application to compute PES experienced by various test atoms and molecules in the vicinity of different clusters proves the transferability of the model not just to clusters of different elements but also to various molecules. The descriptors chosen are invariant to rotation, translation, and permutation yet very simple to compute is one of the most crucial points of the present work.

## Introduction

Clusters, being the system of few atoms, have very different properties than their corresponding atomic and macroscopic analogue.<sup>1-6</sup> Due to the unique arrangement of atoms, the properties of clusters vary substantially with size. This size sensitivity is the key feature of atomic clusters and is reflected in all their properties like, melting,<sup>7-10</sup> their growth pattern,<sup>11</sup> reactivity towards various molecules,<sup>12-19</sup> etc. The reactivity of clusters has been investigated by both experimental and theoretical means.<sup>20-27</sup> Roach *et al.* studied the reaction of anionic  $\text{Al}_{7-73}$  clusters with  $\text{H}_2\text{O}$  molecule.<sup>23,24</sup> They demonstrated that  $\text{Al}_{12}^-$  cluster

adsorbs more than one  $\text{H}_2\text{O}$  molecule, while  $\text{Al}_{13}^-$  does not react with  $\text{H}_2\text{O}$ . The electronic closed shell structure (40 electrons) was considered to be the reason for non-reactivity of  $\text{Al}_{13}^-$ . But,  $\text{Al}_{23}^-$  which is also a closed shell (70 electrons) does react while  $\text{Al}_{20}^-$  which is not a closed shell (61 electrons) does not react with  $\text{H}_2\text{O}$ . Hence this variation in reactivity has geometric rather than electronic origin. By adding an atom in  $\text{Al}_{12}^-$ , the reactivity completely diminishes due to the absence of adjacent Lewis acid-Lewis base active sites in  $\text{Al}_{13}^-$  cluster. In smaller size regime where every atom counts, addition or removal of just an atom dramatically changes its properties. Thus, it becomes very difficult to bring out general trends in this size range. It has been also demonstrated by a few groups that not just size, site also affects the reactivity of clusters.<sup>28,29</sup> And hence, to model the interaction of clusters with an incoming adsorbate, all possible adsorption sites for all the clusters must be scanned, which in turn leads to a prohibitively large number of DFT calculations. To overcome this problem, we have employed data driven algorithms of machine learning to predict the site specific interaction energies for various aluminum clusters. Machine learning is preferred over conventional curve fitting because it brings out the underlying complex relations buried in the data set which are useful in prediction for newer and unseen data points as we will demonstrate in this work.

Use of ML methods in combination with DFT is continuously increasing in the field of materials.<sup>30,31</sup> It is being applied for accelerated materials discovery,<sup>32-34</sup> to understand the underlying electronic structure,<sup>35</sup> to obtain chemical information,<sup>36,37</sup> to predict the potential energy functions<sup>38-45</sup> and so on. Success of any ML model hinges on choosing the right set of descriptors. Descriptors should be such that they can bring out accurate and hidden trends from a data set, and yet be as simple as possible. Thus designing features/descriptors that completely describe the system are very crucial. Lot of efforts are being put in developing fingerprints that systematically relate the structural features of samples to their functional properties in quantitative terms.<sup>46-49</sup> These set of features then find varied applications like finding similarity between two structures,<sup>50-52</sup> finding the structure-activity relation for

various systems,<sup>53-55</sup> screening the chemical space to discover novel materials of desired properties<sup>56,57</sup> or even predict properties for a given material.<sup>58-61</sup> In a study by Hansen *et al.*, they outlined a number of established machine learning techniques and investigated the influence of the molecular representation on ML methods performance. The best methods achieve prediction errors of 3 kcal/mol (0.13 eV) for the atomization energies of a wide variety of molecules.<sup>62</sup>

Few groups have recently used ML for *in silico* design of catalysts and proved the validity of their model against the first principles methods.<sup>63-65</sup> Wang *et al.* recently demonstrated the use of artificial neural networks combined with kinetic analysis for rapid screening of bimetallic catalysts. Through a Machine Learning model, they could capture the underlying complex and non-linear interaction between adsorbate and metal, with reported RMSE  $\sim 0.2$  eV.<sup>64</sup> Another group, Ma *et al.* adopted the use of ML to capture interactions of adsorbate on multimetallics for catalyst screening of CO<sub>2</sub> electroreduction with an RMSE of  $\sim 0.1$  eV.<sup>63</sup> Other studies integrating *ab initio* calculations and ML, for transition metal catalysts screening have reported errors (RMSE) as low as  $\sim 0.12$  eV.<sup>65</sup>

Owing to the excellent catalytic properties, nanoparticles and atomic clusters have always been objects of interest.<sup>66-70</sup> Recently, there is an increasing trend in resorting to ML for discovering correlations between geometric structure and catalytic activities<sup>67,70</sup> of metal surfaces as well as nanoparticles.<sup>66</sup> Recently an ML scheme was proposed to understand catalytic activities based on local atomic configurations and applied to study direct NO decomposition on RhAu alloy nanoparticles.<sup>68</sup> A local structural similarity kernel known as a smooth overlap of atomic positions (SOAP) was used to find similarities between two geometries based on structural descriptors. Gasper *et al.* used the gradient-boosting algorithm, for prediction of CO adsorption energies on Pt clusters.<sup>69</sup> They built predictive models of site-specific adsorbate binding on realistic, low-symmetry nanostructures, with AME  $\sim 0.1$  eV (with respect to DFT). Descriptors used during the training of the ML model in this study comprised of d-band center energy, s and p band center energies, Bader charges, generalized

coordination number, etc.

In the present work, we use both DFT and ML techniques, to predict the interaction energy of Al clusters with H atom as an adsorbate. This interaction is studied as a function of increasing size. DFT investigations bring out the one to one correlation between neighbor distance distribution of atoms in a cluster and their corresponding interaction energy. This strong correlation provides the rationale of choosing distances between adsorbate and the surface atoms of cluster as descriptors to train the ML model. And indeed our model based on ‘only’ distances as descriptors could predict the interaction energy with errors as low as 0.05 eV. Further, the transferability of our ML model is demonstrated by its application to different homogeneous ( $\text{Na}_{10}$ ) as well as bimetallic clusters ( $\text{Al}_6\text{Ga}_6$ ). To validate our model the adsorbate is also replaced by other atoms (N), and molecules ( $\text{N}_2$ ,  $\text{O}_2$ , and CO).

## Computational Details

To determine the overall reactivity of a cluster, site specific interaction energy needs to be evaluated. However, owing to the lack of long range order and highly altered short range order, different atoms within a cluster interact differently with an incoming adsorbate. To quantify this site specific variation, we have computed interaction energy of various atoms like H, N and molecules like  $\text{N}_2$ ,  $\text{O}_2$ , and CO with Al clusters. Also, the interaction of H atom with cluster of another element like  $\text{Na}_{10}$  and bimetallic cluster like  $\text{Al}_6\text{Ga}_6$  was computed. All these resulted into about 35,000 single point calculations. The adsorbates were placed at on-top position of all the surface sites (i.e. surface atoms) for all the clusters with size ranging from 5 to 80. The GS geometries for all the clusters were taken from previously reported work.<sup>71-74</sup> As shown in Fig. 1, the adsorbate was kept along the outward radial vector from center of mass of the cluster to surface atom. The distance of adsorbate was varied between 1.30 Å to 3.00 Å from the surface site. All the calculations were carried out within the Kohn-Sham formulation of DFT. Projector Augmented Wave pseudopotential<sup>75,76</sup> was

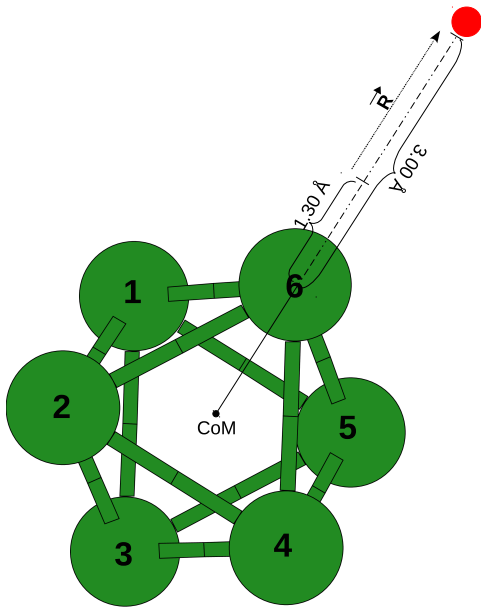


Figure 1:  $\text{Al}_6$  cluster is shown with center of mass marked at the center. The adsorbate is placed along the radial vector pointing outwards from the center of mass to surface atom. Distance between adsorbate and surface atom is varied from 1.30 Å to 3.00 Å.

used, with Perdew–Burke–Ehrzenhof (PBE)<sup>77</sup> approximation for the exchange–correlation and generalized gradient<sup>78</sup> approximation, as implemented in plane wave pseudo potential based code, *VASP*.<sup>79–81</sup> Cubic simulation cell, with the image in each cell separated by at least 15 Å of vacuum, was used. Energy convergence criteria of  $10^{-5}$  eV was used for SCF calculations.

Data collected from DFT calculations was then used to train a ML model. We used the Gradient Boosting Regression (GBR) algorithm as implemented in the scikit-learn python package.<sup>82</sup> GBR is a regression technique that uses decision tree based classifiers as weak learners. We used the mean squared error function as our loss function (i.e. the objective function to be optimized). The GBR was selected after comparing it against four other regression algorithms viz. Linear Regression, Ridge Regression, LASSO and Stochastic Gradient Descent (SGD). An exhaustive grid search was carried out to find the best parameter values of an estimator. 5-fold cross validation was performed to test accuracy of the model. AME was used as the scoring parameter during cross validation. Multiple checks like plotting the validation curve and learning curves were used to ensure that the model did not

overfit the data.

## Results and Discussion

In clusters, due to the finiteness of the system, every atom does not experience identical environment unlike atoms in bulk. To quantify this variation, nearest neighbor distribution of every atom in all the clusters was studied. In this distribution, distance ( $d_{i,j}$ ) between every pair of atom  $i$  and  $j$  in a cluster was calculated. Fig. 2-(a) shows the geometry of  $\text{Al}_{13}$  cluster. The corresponding  $13 \times 13$  distance matrix for  $\text{Al}_{13}$  is shown in Fig. 2-(b). To identify the atoms that experienced identical environment (in terms of neighbor distances), distances were arranged in ascending order in the sorted distance matrix as shown in Fig. 2-(c). A careful look at this matrix revealed that there were only two unique rows. Implying that all the twelve surface atoms in  $\text{Al}_{13}$  were grouped in two classes as is also seen in Fig. 2-(d). Similarly, for  $\text{Al}_{12}$  cluster, eleven surface atoms were grouped into seven classes as shown in Fig. 2-(e-h). It should be noted that upon addition of just one atom in  $\text{Al}_{12}$  cluster, seven different classes merge and form only two classes in the case of  $\text{Al}_{13}$ , i.e. an asymmetric cluster gets transformed into a highly symmetric one. As evident from the Fig. 2-(d) and Fig. 2-(h), the interatomic distances can be used to indicate how (dis)ordered the cluster is. By ‘ordered’ cluster we mean a cluster with many identical atoms in terms of the chemical environment that they experience. For example,  $\text{Al}_{13}$ , and  $\text{Al}_{36}$  are ‘ordered’ clusters because all the surface atoms are grouped into 2 for  $\text{Al}_{13}$  as shown in Fig. 2-(d), and 6 for  $\text{Al}_{36}$  classes as shown in Fig. 3-(a). Whereas for all the disordered clusters, more than half of surface atoms experience unique environment like 7 in case of  $\text{Al}_{12}$  as shown in Fig. 2-(h) and 23 in  $\text{Al}_{25}$  as shown in Fig. 3-(b).

This variation in the arrangement of individual atoms is a characteristic of atomic clusters in this size regime. As noted earlier, Roach *et al.* demonstrated a substantial change in the reactivity of  $\text{Al}_{12}^-$  compared to  $\text{Al}_{13}^-$  cluster towards  $\text{H}_2\text{O}$  molecule.<sup>23,24</sup> A proof of concept

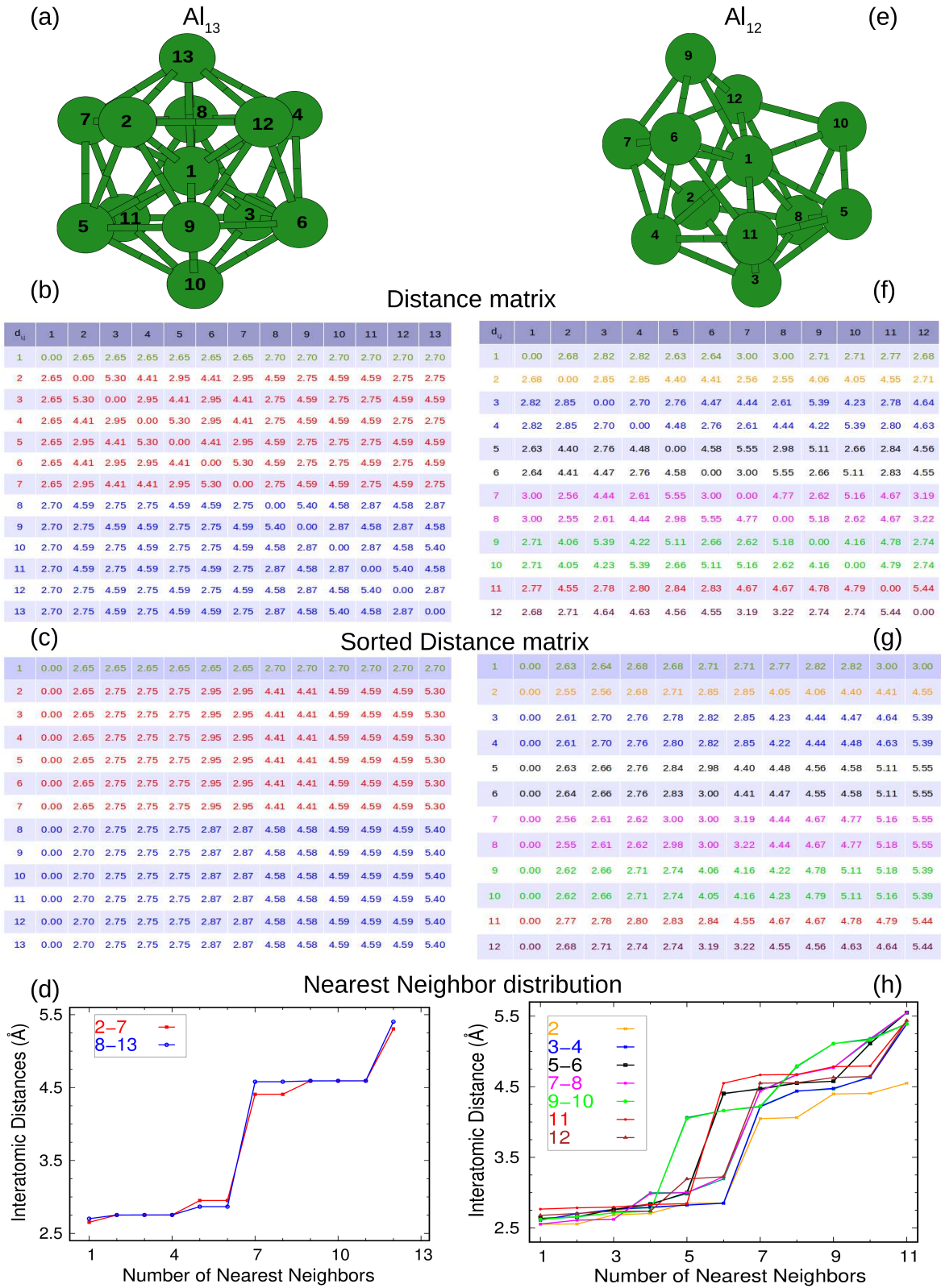


Figure 2: (a) Geometry of  $Al_{13}$  cluster, (b) Distance matrix(DM) of  $Al_{13}$  where atoms experiencing identical environment are shown in same color, (c) Sorted Distances in each row of DM, (d) Nearest Neighbor (NN) distribution for  $Al_{13}$  showing two distinct lines. (e) Geometry of  $Al_{12}$  cluster, (f) DM of  $Al_{12}$  where atoms experiencing identical environment are shown in same color, (g) Sorted Distances in each row of DM, (h) NN distribution for  $Al_{12}$  showing seven distinct lines. NN distribution for the core atoms is not shown.



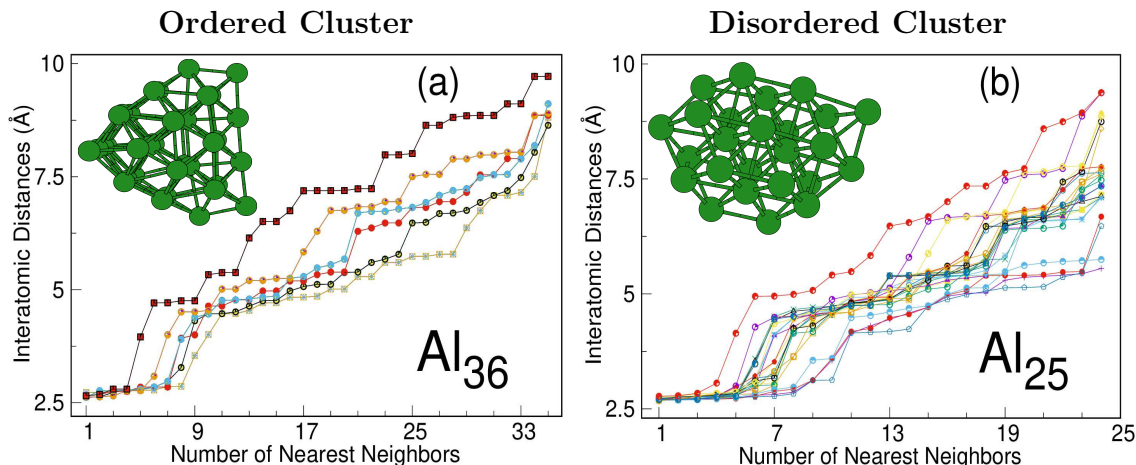


Figure 3: Figure shows variation in the interatomic distances as function of nearest neighbors for all surface atoms. (a) shows the ‘ordered’  $\text{Al}_{36}$  cluster, having 32 surface atoms which are grouped into six different classes. (b) shows ‘disordered’  $\text{Al}_{25}$  cluster. In this cluster, there are 23 surface atoms, all of these atoms have different distance distribution. Only the distances of surface atoms are shown in NN distribution. The inset figure shows the geometry of respective clusters.

for such experimental studies on reactivity lies in our observation based on a significant change in the symmetry of clusters with addition of just one atom as shown in Fig. 2-(d) and Fig. 2-(h). It brings out the fact that variation in behavior of clusters with changing size originates from their geometries. And hence, motivation of our work lies on understanding the interaction of clusters with incoming adsorbates as a function of changing geometries with size (fixed geometry for a size). In our work, cluster geometries were expressed in terms of the nearest neighbor distribution. We demonstrate that the site specific interaction depends upon the nearest neighbor distribution of that specific atom (or site) within a cluster.

All atoms having identical nearest neighbor distribution within a cluster, interact identically with the incoming adsorbate. To elaborate this point further, in Fig. 4 we show the interaction energies for all the atoms within a cluster, for a few representative sizes along with their nearest neighbor distribution (or interatomic distances) in the inset. In the case of  $\text{Al}_{13}$  (see inset of Fig. 4-a) as explained earlier all the surface atoms could be grouped in two classes based on their respective interatomic distances, indicating that an incoming adsorbate would experience only ‘two’ different environments. Further, when interaction energy of these surface atoms with an H atom (as adsorbate) was computed, it was observed that atoms belonging to one class interact identically with the adsorbate, resulting into iden-

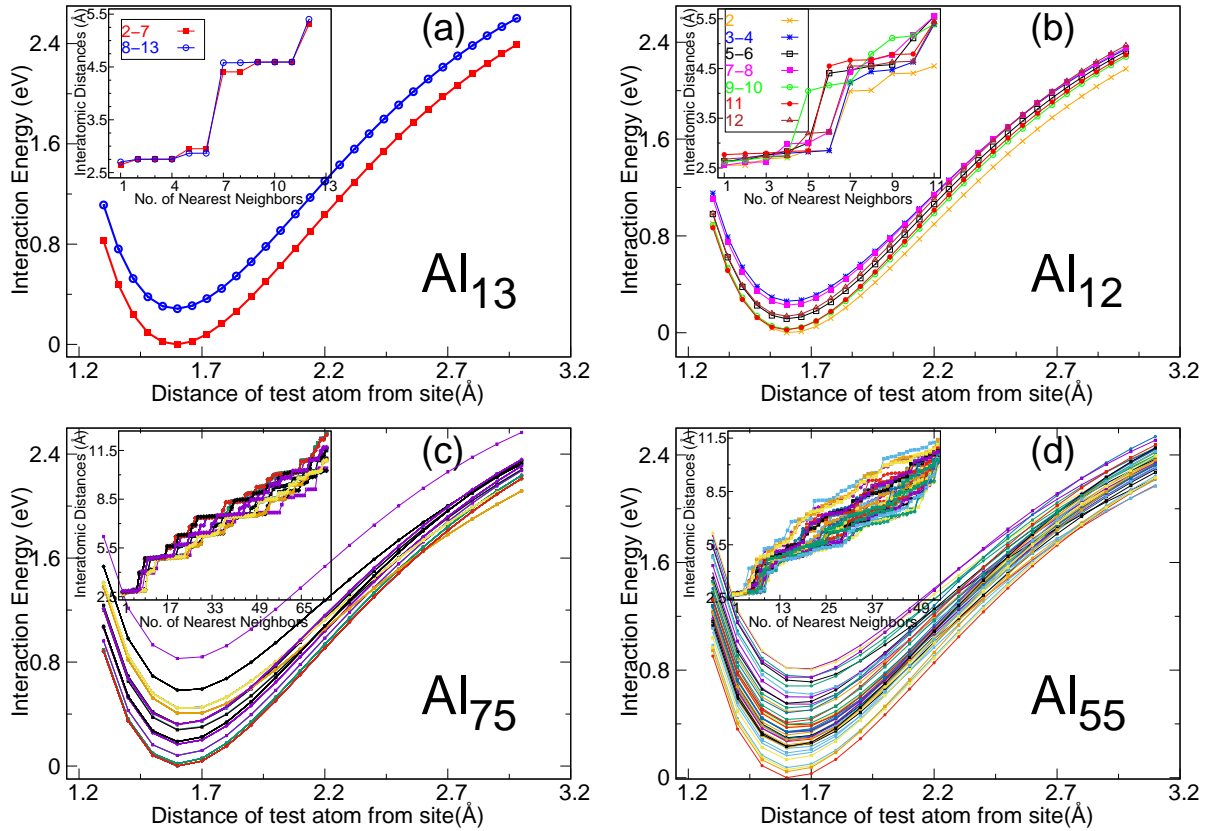


Figure 4: The figure shows distance dependent interaction energy of all surface atoms for a few representative clusters. Atoms with identical nearest neighbor distribution also exhibit identical interaction energy pattern towards an H atom. Inset figure shows variation in the interatomic distances as function of nearest neighbors for all surface atoms of these clusters.

tical interaction energy as shown in Fig. 4-(a). This is evident from the interaction energy of the adsorbate with all the surface atoms when placed at ‘on top’ position. This one to one correlation between identical nearest neighbor distribution and interaction energy is also observed in larger clusters like  $Al_{75}$  and  $Al_{55}$  as shown in Fig. 4-(c) and 4-(d) respectively.

It has been also observed that two sites result into identical interaction energy pattern, if and only if ‘all’ the interatomic distances are identical. For example, in the case of  $Al_9$ , for two atoms, their first 6 nearest neighbors are at identical distances and the last two distances differ as shown in Fig. 5. However, it has resulted into two distinct interaction energy patterns for the respective atoms as shown in inset of Fig. 5. This one to one correlation between the nearest neighbor distances and interaction energy pattern is observed in all the Al clusters that we have studied with size ranging from 5 to 80. The same trend was

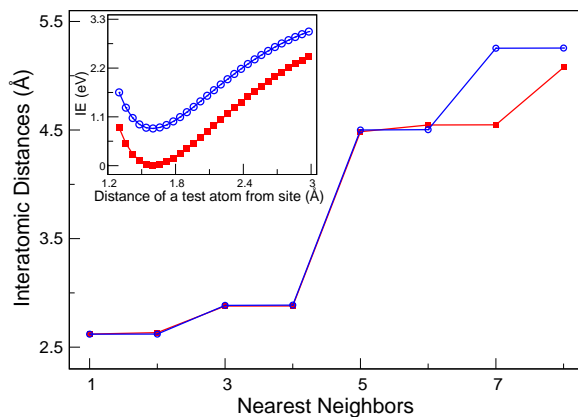


Figure 5: The figure shows nearest neighbor distribution for two surface atoms of  $\text{Al}_9$  cluster. The inset shows distance dependent interaction energy for these two atoms. Two sites (or surface atoms) have identical interaction energy if and only if they have identical chemical environment defined in terms of all interatomic distances.

observed when H atom was replaced with N atom, and  $\text{N}_2$ ,  $\text{O}_2$ , and CO molecules. Also, when the cluster is replaced with that of other elements like  $\text{Na}_{10}$ , and for bimetallic cluster like  $\text{Al}_6\text{Ga}_6$ , this correlation holds. This strong correlation between identical adsorption sites and identical interaction energy can be understood from the perspective of Hohenberg-Kohn's first theorem. HK's first theorem describes the one to one correspondence between external potential and charge density and hence energy (a functional of charge density). Identical sites are the ones that have same relative distribution of atoms in the cluster i.e. identical nearest neighbor distribution. Which in turn results into identical external potential when a test atom is placed at appropriate position (as described in computational details) and hence, identical interaction energy.

Establishing a structure-property relation to understand reactivity problems better will greatly reduce DFT based computational efforts. But, coming up with a set of descriptors that have characteristics like transferability, universality, potential to capture accurate trends and yet be simple is still an ongoing area of research. And so, it will be interesting to test if this one-to-one correlation between nearest neighbor distribution and interaction energy could be exploited by employing data driven models at a minimal computational cost. Since in this size regime, properties of clusters vary substantially by addition/removal of just an atom, it becomes important to study the interaction of clusters as a function of size. The size

and site specific interaction energy data generated through our extensive DFT computations was used to train the ML model. The data was fed to GBR to predict the interaction energies for all unique adsorption sites of the clusters between 5 to 20 and few selected larger clusters (25, 36, 42, 55, 67, and 75). This is a balanced mixture of ordered and disordered clusters. Taking a hint from the DFT investigations, descriptors that captured this structure-property relation were designed. While modelling the interaction of clusters with adsorbate the (dis)similarity between two adsorption sites had to be captured. And hence, nearest neighbor distribution as seen by the adsorbate was the logical choice of descriptors. The chosen set of descriptors did not represent any homometric pairs as the cluster geometries were fixed, while only the distance between adsorbate and cluster varied. For homogeneous clusters, only distances were used as descriptors while nuclear charge was also included for bimetallic cluster.

**Table 1: Absolute Mean Errors (AME) as a function of descriptors (interatomic distances (nn)) are shown in the table for various clusters. As seen from the table, increasing representation of the system results into improved accuracy. The overall error is 0.05 eV.**

Cluster		AME as a function of (nearest neighbors as) descriptors										
size	nn2	nn3	nn4	nn5	nn6	nn7	nn8	nn9	nn10	nn11	nn12	nn13
5	0.085	0.084	0.050	0.050								
6	0.034	0.035	0.035	0.034	0.032							
7	0.179	0.180	0.178	0.059	0.051	0.051						
8	0.057	0.038	0.035	0.029	0.028	0.028	0.028					
9	0.226	0.228	0.219	0.133	0.127	0.122	0.055	0.054				
10	0.051	0.053	0.051	0.052	0.051	0.044	0.043	0.043	0.044			
11	0.281	0.268	0.194	0.169	0.114	0.096	0.096	0.079	0.060	0.060		
12	0.081	0.069	0.067	0.063	0.055	0.041	0.041	0.039	0.038	0.038	0.032	
13	0.131	0.132	0.130	0.082	0.083	0.086	0.026	0.026	0.026	0.025	0.024	0.021

A trend of reducing prediction errors with increasing system representation was seen for all the clusters that we had studied. For any surface site of an n atom cluster, there will be n

distances as descriptors. These descriptors were distances from adsorbate to all the atoms in a cluster and hence invariant to rotation, translation, and permutation of the system. Since, the cluster geometries are always fixed for any given size,  $n$  distances are enough to represent the entire system and hence the external potential. The model was trained each time by gradually including more descriptors i.e. distances. In Tab. 1 we list the variation in AME as a function of increasing number of descriptors for smaller cluster sizes. The variation in AME is correlated with interatomic distances from the H atom. We will discuss this further by closely analyzing the specific case of  $\text{Al}_{13}$ . In Fig. 6-(a) we have plotted the AME as a

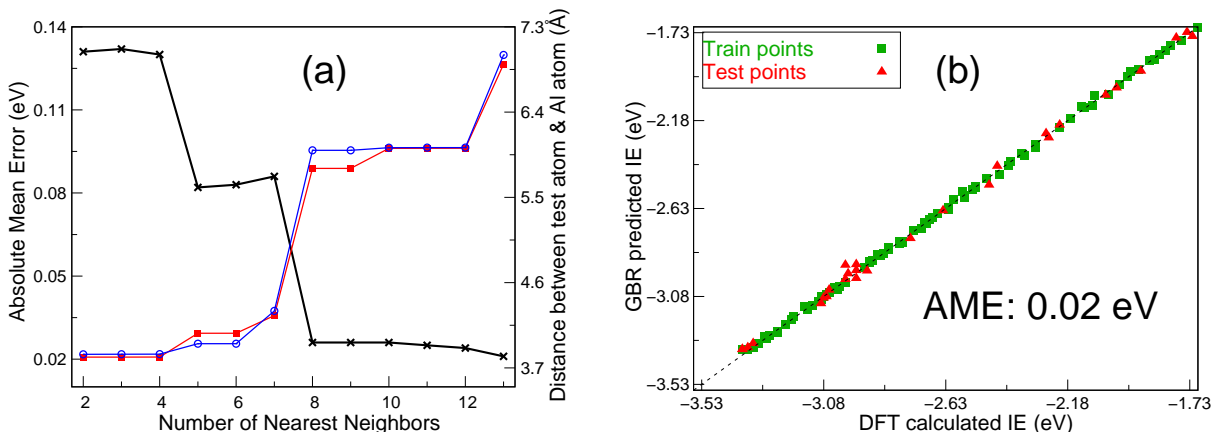


Figure 6: (a) shows the decrease of errors (AME) with increasing number of descriptors for the  $\text{Al}_{13}$  cluster plotted on y1 axis. We have used the distance between H atom and surface atoms as descriptors which is plotted on y2 axis. It is seen in figure that as the two groups in  $\text{Al}_{13}$  are distinguished in NN distribution, the error reduces. (b) shows absolute mean error in interaction energy prediction by ML model with reference to DFT.

function of number of descriptors (number of NN distances from the surface site) used to fit the model for predicting interaction energies for  $\text{Al}_{13}$ . As noted earlier,  $\text{Al}_{13}$  has only two types of atoms. The difference between these two types of atoms in their nearest neighbor distribution is picked up in the ML model. And hence we observed improvement in AME at distances where these two groups differ from each other i.e. AME reduced from 0.13 eV to 0.08 eV with descriptors up to nn4 versus nn5. A similar jump (decrease) in AME was observed when nn8 was also included as shown in Tab. 1. nn8 is the point at which the two classes further separated. In Fig. 6-(b) ML predicted energies for  $\text{Al}_{13}$  are plotted against DFT calculated energies. The AME in this specific case is 0.02 eV. This correlation between reduction in AME and variation in the nearest neighbor distribution was also observed for

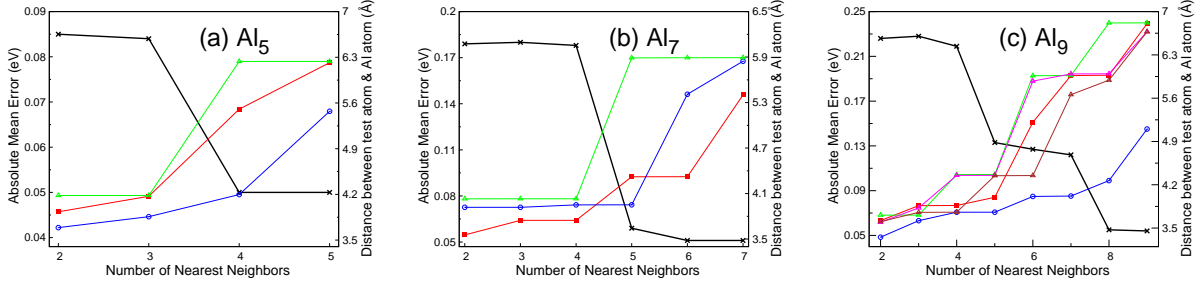


Figure 7: Figure shows the decrease of errors (AME) with increasing number of descriptors for the clusters plotted on y1 axis. We have used the distance between H atom and surface atoms as descriptors which is plotted on y2 axis.

$Al_5$ ,  $Al_7$ , and  $Al_9$  clusters (see Tab. 1). The nearest neighbor distribution and variation in AME plots for the above mentioned cases are shown in Fig. 7. Overall, the machine learning model has picked up the underlying correlation between nearest neighbor distances and interaction energy. As has been discussed, by means of distances as descriptors, we are providing information about the external potential and thus catching the essence of Hohenberg-Kohn’s first theorem.

**Table 2:** Absolute mean errors (AME) as function of descriptors (interatomic distances (nn)) are shown in the table for larger clusters. The last three columns present 25%, 50%, and 100% of the system representation respectively. The numbers in the brackets indicate the number of interatomic distances used to predict the interaction energy.

Cluster	AME as a function of nearest neighbors as descriptors							
size	nn2	nn3	nn4	nn5	nn10	nn 25%	nn 50%	nn 100%
25	0.137	0.111	0.113	0.107	0.071	0.095(6)	0.067(13)	0.068(24)
36	0.063	0.050	0.054	0.056	0.044	0.045(9)	0.044(18)	0.030 (35)
42	0.083	0.084	0.077	0.074	0.076	0.076(11)	0.069(21)	0.059(41)
55	0.125	0.110	0.104	0.100	0.090	0.090(14)	0.088(28)	0.086(54)
67	0.083	0.077	0.072	0.066	0.048	0.048(17)	0.045(35)	0.049(66)
75	0.119	0.125	0.100	0.081	0.081	0.080 (18)	0.071(37)	0.060(74)

This correlation between nearest neighbor and variation in AME is strikingly evident and easy to capture in smaller clusters. While it is not so clear in the case of larger cluster due to increased complexity of the systems. And this is what reflects into the AME as a function of descriptors as shown in Tab. 2. It was observed that the variation in AME was inconsistent

when descriptors up to nn10 versus all distances (nn100%) were used. For example, in the case of  $\text{Al}_{36}$  and  $\text{Al}_{75}$ , reduction in AME was more than 25% for each of them as shown in Tab. 2. It must be noted that  $\text{Al}_{36}$  (see Fig. 3-(a)) and  $\text{Al}_{75}$  (see Fig. 4-(c)) are highly symmetric clusters. Whereas for asymmetric clusters like  $\text{Al}_{25}$ ,  $\text{Al}_{55}$ , and  $\text{Al}_{67}$  the reduction in errors were less than 5% as evident from Tab. 2. But for another asymmetric cluster,  $\text{Al}_{42}$ , the reduction is much larger i.e. about 20% which is similar to that of symmetric clusters. Thus generalization of results becomes difficult for larger clusters. Nonetheless, even for larger clusters the one to one correlation between reduction in AME and increasing system representation still holds. The overall AME reported in our work is  $\approx 0.05$  eV.

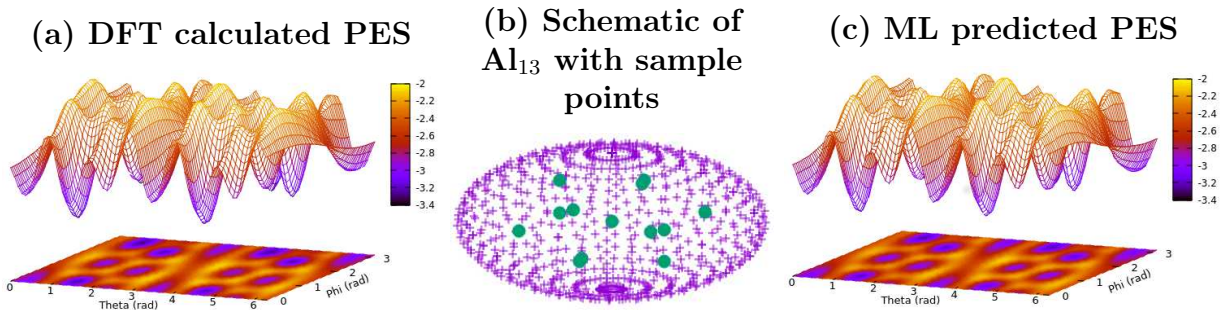


Figure 8: (a) PES computed through DFT calculations. (b) cartoon of  $\text{Al}_{13}$  cluster and points selected on a sphere to compute interaction of adsorbate with cluster. (c) ML generated PES. It is evident that our model has picked up the variation in PES quite faithfully.

Since the line of search for all the results discussed above was restricted along the radial vector, to model a real situation wherein an adsorbate can approach the cluster from any direction, all possible directions had to be scanned. The one to one correlation between identical sites and identical interaction would be difficult to quantify for this situation, as now the adsorbate was not placed only at on-top sites. Nonetheless, the same recipe of descriptors was still legitimate as the distances taken were from the adsorbate to the atoms representing the external potential. And so, the same set of descriptors would capture the change in chemical environment as seen by an incoming adsorbate. Thus, a logical proposition is, the potential energy surface (PES) of an adsorbate in the vicinity of a cluster could be explored with our model. To validate this, we scanned PES at 800 different points (in all possible directions) around a cluster and is shown in Fig 8. We computed the interaction energy of

H atom for these randomly selected 800 points on a sphere that enclosed the  $\text{Al}_{13}$  cluster at its center (see Fig. 8-(b)). The distance of H atom from the closest surface site of cluster varies between 1.60 Å to 2.69 Å. This result is particularly important because through this we could predict interaction energy at any point on the PES of the cluster-adsorbate system with AME as low as 0.04 eV. The success of ML model, in this case, is a proof of concept

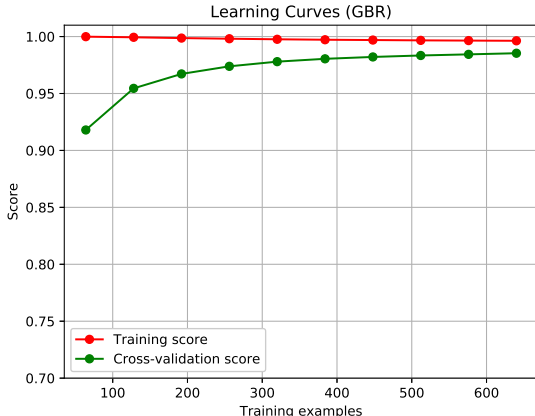


Figure 9: It is evident from the learning curve that the training score is maximum and cross validation score increases gradually with increasing data points.

that nearest neighbor distances are the correct choice of descriptors. It was also found that with only 400 points on the sphere we could achieve same level of accuracy as with 800 points as shown in learning curve Fig. 9. Further as seen from the figure, our model has picked up variation in PES quite faithfully. The minima on the PES represents on-top position which is the most favorable position for the H atom on this surface. Whereas the maxima is the least favorable position and turns out to be a bridge position for the H atom.

To further validate our model we tested it on other clusters like  $\text{Na}_{10}$  and  $\text{Al}_6\text{Ga}_6$ . It was observed that for H atom adsorbed on a highly asymmetric  $\text{Na}_{10}$  cluster, our ML model with the same recipe of descriptors predicted the IE with AME  $\approx 0.038$  eV. To demonstrate the universality of our work, calculations performed with different adsorbing species on Al clusters are noted below. When a single N atom was adsorbed at on-top positions on  $\text{Al}_{13}$  cluster, not only the one to one correlation was observed again but also the AME from ML model was 0.06 eV, i.e. in same range as our previous results. Further the errors for prediction



of IE using the same ML model when molecules like  $N_2$ ,  $O_2$ , and CO were adsorbed on  $Al_{12}$  turned out to be, 0.045 eV, 0.049 eV, and 0.042 eV respectively. Finally, we also tested the validity of our ML model on bimetallic cluster  $Al_6Ga_6$ . AME for an H atom adsorbed on top of this cluster turned out to be 0.09 eV. This error was obtained based on only structural representation of the cluster. With the inclusion of nuclear charge/ionic radii of both the elements of the cluster, viz. Al and Ga, in the descriptor set, the AME got down to 0.058 eV.

In a nutshell, the descriptors used to train the ML model are as simple as distances between adsorbate and the surface atoms correlating the structure and activity between the two. Successful prediction of interaction energy by means of descriptors that systematically represent the external potential catches the essence of Hohenberg-Kohn’s first theorem. Our approach differs from the previous work in a few key ways: 1. Descriptors chosen were such so as to model the interaction of a cluster and an incoming adsorbate. And hence, the chemical environment that an adsorbate experienced was explored, 2. The descriptors used did not represent any homometric pairs as only unique adsorption sites for fixed cluster geometries were used and finally 3. The ML model was trained on purely the structural representation of the cluster.

## Conclusion

To summarize we have combined DFT with ML to understand the interaction between an adsorbate and clusters. The key results of the present work are as follows: 1. Our extensive DFT calculations establish a one-to-one correlation between the nearest neighbor distances and interaction energy for small Al clusters. The results, as demonstrated, are generic and applicable to all the clusters and different adsorbates. 2. We employ the GBR model to predict the site specific interaction energies by using ‘only’ interatomic distances as descriptors. The absolute mean errors are about 0.05 eV. With this, we also demonstrate

that our ML algorithm picks up the one-to-one correlation between the nearest neighbor distribution and the site specific interaction energies and hence essence of Hohenberg-Kohn's first theorem. 3. We reproduce the PES for a test atom in the vicinity of the cluster by employing our ML model. To get AME about as low as 0.04 eV we require only 400 single point calculations, which demonstrates that we could circumvent the compute intensive DFT by employing this model. 4. Our descriptors are the interatomic distances, and hence the computational cost is negligible. In conclusion, we designed a set of descriptors that were as simple as nearest neighbor distances and yet the ones that could accurately capture the structure-activity relation between the cluster and adsorbate.

## Acknowledgements

The authors thank Dr. Leelavati Narlikar for fruitful discussions. CSIR-4PI is gratefully acknowledged for the computational facility. KJ acknowledges DST (EMR/2016/000591) for partial financial support. SM acknowledges UGC for research fellowship. SA acknowledges DST-INSPIRE for research fellowship.

## References

- (1) Jortner, J. Cluster size effects. *Zeitschrift für Physik D Atoms, Molecules and Clusters* **1992**, *24*, 247–275.
- (2) Sanchez, A.; Abbet, S.; Heiz, U.; Schneider, W.-D.; Häkkinen, H.; Barnett, R. N.; Landman, U. When Gold Is Not Noble: Nanoscale Gold Catalysts. *J. Phys. Chem. A* **1999**, *103*, 9573–9578.
- (3) Jena, P.; Castleman, A. W. Clusters: A bridge across the disciplines of physics and chemistry. *Proc. Natl. Acad. Sci.* **2006**, *103*, 10560–10569.

- (4) Castleman Jr, A.; Khanna, S. Clusters, superatoms, and building blocks of new materials. *J. Phys. Chem. C* **2009**, *113*, 2664–2675.
- (5) Alonso, J. A. *Structure and properties of atomic nanoclusters*; World Scientific, 2012.
- (6) Berry, R. S.; Smirnov, B. M. Bridging the macro and micro. *Chem. Phys. Lett* **2013**, *573*, 1–4.
- (7) Schmidt, M.; Kusche, R.; von Issendorff, B.; Haberland, H. Irregular variations in the melting point of size-selected atomic clusters. *Nature* **1998**, *393*, 238.
- (8) Breaux, G. A.; Hillman, D. A.; Neal, C. M.; Benirschke, R. C.; Jarrold, M. F. Gallium Cluster “Magic Melters”. *J. Am. Chem. Soc.* **2004**, *126*, 8628.
- (9) Joshi, K.; Krishnamurty, S.; Kanhere, D. “Magic melters” have geometrical origin. *Phys. Rev. Lett.* **2006**, *96*, 135703.
- (10) Berry, R. S.; Smirnov, B. M. Configurational transitions in processes involving metal clusters. *Phys. Rep* **2013**, *527*, 205–250.
- (11) Shvartsburg, A. A.; Jarrold, M. F. Tin clusters adopt prolate geometries. *Phys. Rev. A* **1999**, *60*, 1235.
- (12) Cox, D.; Trevor, D.; Whetten, R.; Kaldor, A. Aluminum clusters: ionization thresholds and reactivity toward deuterium, water, oxygen, methanol, methane, and carbon monoxide. *J. Phys. Chem.* **1988**, *92*, 421–429.
- (13) Argo, A.; Odzak, J.; Lai, F.; Gates, B. Observation of ligand effects during alkene hydrogenation catalysed by supported metal clusters. *Nature* **2002**, *415*, 623–626.
- (14) Fu, Q.; Saltsburg, H.; Flytzani-Stephanopoulos, M. Active nonmetallic Au and Pt species on ceria-based water-gas shift catalysts. *Science* **2003**, *301*, 935–938.

- (15) Campbell, C. T. The active site in nanoparticle gold catalysis. *Science* **2004**, *306*, 234–235.
- (16) Chen, M.; Goodman, D. The structure of catalytically active gold on titania. *Science* **2004**, *306*, 252–255.
- (17) Lemire, C.; Meyer, R.; Shaikhutdinov, S.; Freund, H.-J. Do quantum size effects control CO adsorption on gold nanoparticles? *Angew. Chem.* **2004**, *43*, 118–121.
- (18) Wei, J.; Iglesia, E. Mechanism and site requirements for activation and chemical conversion of methane on supported Pt clusters and turnover rate comparisons among noble metals. *J. Phys. Chem. B* **2004**, *108*, 4094–4103.
- (19) Vajda, S.; Pellin, M. J.; Greeley, J. P.; Marshall, C. L.; Curtiss, L. A.; Ballentine, G. A.; Elam, J. W.; Catillon-Mucherie, S.; Redfern, P. C.; Mehmood, F. et al. Subnanometre platinum clusters as highly active and selective catalysts for the oxidative dehydrogenation of propane. *Nat. Mater.* **2009**, *8*, 213–216.
- (20) Heiz, U.; Vanolli, F.; Sanchez, A.; Schneider, W.-D. Size-dependent molecular dissociation on mass-selected, supported metal clusters. *J. Am. Chem. Soc.* **1998**, *120*, 9668–9671.
- (21) Wallace, W. T.; Whetten, R. L. Carbon monoxide adsorption on selected gold clusters: highly size-dependent activity and saturation compositions. *J. Phys. Chem. B* **2000**, *104*, 10964–10968.
- (22) Cao, B.; Starace, A. K.; Judd, O. H.; Jarrold, M. F. Melting Dramatically Enhances the Reactivity of Aluminum Nanoclusters. *J. Am. Chem. Soc.* **2009**, *131*, 2446–2447.
- (23) Roach, P. J.; Woodward, W. H.; Castleman, A.; Reber, A. C.; Khanna, S. N. Complementary active sites cause size-selective reactivity of aluminum cluster anions with water. *Science* **2009**, *323*, 492–495.

- (24) Reber, A. C.; Khanna, S. N.; Roach, P. J.; Woodward, W. H.; Castleman Jr, A. Reactivity of aluminum cluster anions with water: origins of reactivity and mechanisms for H<sub>2</sub> release. *J. Phys. Chem. A* **2010**, *114*, 6071–6081.
- (25) Kulkarni, B. S.; Krishnamurty, S.; Pal, S. Size- and Shape-Sensitive Reactivity Behavior of Al<sub>n</sub> (n = 2–5, 13, 30, and 100) Clusters Toward the N<sub>2</sub> Molecule: A First-Principles Investigation. *J. Phys. Chem. C* **2011**, *115*, 14615–14623.
- (26) Yin, S.; Bernstein, E. R. Gas phase chemistry of neutral metal clusters: distribution, reactivity and catalysis. *Int. J. Mass Spectrom.* **2012**, *321*, 49–65.
- (27) Luo, Z.; Castleman Jr, A.; Khanna, S. N. Reactivity of metal clusters. *Chem. Rev.* **2016**, *116*, 14456–14492.
- (28) Das, S.; Pal, S.; Krishnamurty, S. Understanding the site selectivity in small-sized neutral and charged Al<sub>n</sub> (4 ≤ n ≤ 7) clusters using density functional theory based reactivity descriptors: a validation study on water molecule adsorption. *J. Phys. Chem. A* **2013**, *117*, 8691–8702.
- (29) Luo, Z.; Smith, J. C.; Berkdemir, C.; Castleman, A. Gas-phase reactivity of aluminum cluster anions with ethanethiol: Carbon–sulfur bond activation. *Chem. Phys. Lett.* **2013**, *590*, 63–68.
- (30) Mueller, T.; Kusne, A. G.; Ramprasad, R. Machine learning in materials science: Recent progress and emerging applications. *Reviews in Computational Chemistry* **2016**, *29*, 186–273.
- (31) Butler, K. T.; Davies, D. W.; Cartwright, H.; Isayev, O.; Walsh, A. Machine learning for molecular and materials science. *Nature* **2018**, *559*, 547.
- (32) Hautier, G.; Fischer, C. C.; Jain, A.; Mueller, T.; Ceder, G. Finding nature’s missing

- ternary oxide compounds using machine learning and density functional theory. *Chem. Mater.* **2010**, *22*, 3762–3767.
- (33) Pilania, G.; Wang, C.; Jiang, X.; Rajasekaran, S.; Ramprasad, R. Accelerating materials property predictions using machine learning. *Sci. Rep.* **2013**, *3*, 2810.
- (34) Meredig, B.; Agrawal, A.; Kirklin, S.; Saal, J. E.; Doak, J.; Thompson, A.; Zhang, K.; Choudhary, A.; Wolverton, C. Combinatorial screening for new materials in unconstrained composition space with machine learning. *Phys. Rev. B* **2014**, *89*, 094104.
- (35) Takigawa, I.; Shimizu, K.-i.; Tsuda, K.; Takakusagi, S. Machine-learning prediction of the d-band center for metals and bimetals. *RSC Adv.* **2016**, *6*, 52587–52595.
- (36) Ulissi, Z. W.; Medford, A. J.; Bligaard, T.; Nørskov, J. K. To address surface reaction network complexity using scaling relations machine learning and DFT calculations. *Nat. Comm.* **2017**, *8*, 14621.
- (37) Bose, S.; Dhawan, D.; Nandi, S.; Sarkar, R. R.; Ghosh, D. Machine learning prediction of interaction energies in rigid water clusters. *Physical Chemistry Chemical Physics* **2018**, *20*, 22987–22996.
- (38) Bukkapatnam, S.; Malshe, M.; Agrawal, P.; Raff, L.; Komanduri, R. Parametrization of interatomic potential functions using a genetic algorithm accelerated with a neural network. *Phys. Rev. B* **2006**, *74*, 224102.
- (39) Morawietz, T.; Behler, J. A density-functional theory-based neural network potential for water clusters including van der waals corrections. *J. Phys. Chem. A* **2013**, *117*, 7356–7366.
- (40) Natarajan, S. K.; Morawietz, T.; Behler, J. Representing the potential-energy surface of protonated water clusters by high-dimensional neural network potentials. *Phys. Chem. Chem. Phys.* **2015**, *17*, 8356–8371.

- (41) Manzhos, S.; Dawes, R.; Carrington, T. Neural network-based approaches for building high dimensional and quantum dynamics-friendly potential energy surfaces. *Int. J. Quantum Chem.* **2015**, *115*, 1012–1020.
- (42) Kolb, B.; Zhao, B.; Li, J.; Jiang, B.; Guo, H. Permutation invariant potential energy surfaces for polyatomic reactions using atomistic neural networks. *J. Chem. Phys.* **2016**, *144*, 224103.
- (43) Dragoni, D.; Daff, T. D.; Csányi, G.; Marzari, N. Achieving DFT accuracy with a machine-learning interatomic potential: Thermomechanics and defects in bcc ferromagnetic iron. *Phys. Rev. Mater.* **2018**, *2*, 013808.
- (44) Jeong, W.; Lee, K.; Yoo, D.; Lee, D.; Han, S. Toward Reliable and Transferable Machine Learning Potentials: Uniform Training by Overcoming Sampling Bias. *J. Phys. Chem. C* **2018**, *122*, 22790–22795.
- (45) Zhang, Y.-J.; Khorshidi, A.; Kastlunger, G.; Peterson, A. A. The potential for machine learning in hybrid QM/MM calculations. *J. Chem. Phys.* **2018**, *148*, 241740.
- (46) Le, T.; Epa, V. C.; Burden, F. R.; Winkler, D. A. Quantitative structure–property relationship modeling of diverse materials properties. *Chem. Rev* **2012**, *112*, 2889–2919.
- (47) Schütt, K.; Glawe, H.; Brockherde, F.; Sanna, A.; Müller, K.; Gross, E. How to represent crystal structures for machine learning: Towards fast prediction of electronic properties. *Phys. Rev. B* **2014**, *89*, 205118.
- (48) Von Lilienfeld, O. A.; Ramakrishnan, R.; Rupp, M.; Knoll, A. Fourier series of atomic radial distribution functions: A molecular fingerprint for machine learning models of quantum chemical properties. *Int. J. Quantum Chem.* **2015**, *115*, 1084–1093.

- (49) Seko, A.; Hayashi, H.; Nakayama, K.; Takahashi, A.; Tanaka, I. Representation of compounds for machine-learning prediction of physical properties. *Phys. Rev. B* **2017**, *95*, 144110.
- (50) Rupp, M.; Tkatchenko, A.; Müller, K.-R.; Von Lilienfeld, O. A. Fast and accurate modeling of molecular atomization energies with machine learning. *Phys. Rev. Lett.* **2012**, *108*, 058301.
- (51) Faber, F. A.; Hutchison, L.; Huang, B.; Gilmer, J.; Schoenholz, S. S.; Dahl, G. E.; Vinyals, O.; Kearnes, S.; Riley, P. F.; Von Lilienfeld, O. A. Prediction errors of molecular machine learning models lower than hybrid DFT error. *J. Chem. Theory Comput.* **2017**, *13*, 5255–5264.
- (52) Bartók, A. P.; De, S.; Poelking, C.; Bernstein, N.; Kermode, J. R.; Csányi, G.; Ceriotti, M. Machine learning unifies the modeling of materials and molecules. *Sci. Adv* **2017**, *3*, e1701816.
- (53) Davran-Candan, T.; Günay, M. E.; Yildirim, R. Structure and activity relationship for CO and O<sub>2</sub> adsorption over gold nanoparticles using density functional theory and artificial neural networks. *J. Chem. Phys.* **2010**, *132*, 174113.
- (54) Jäger, M. O.; Morooka, E. V.; Canova, F. F.; Himanen, L.; Foster, A. S. Machine learning hydrogen adsorption on nanoclusters through structural descriptors. *npj Comput. Mater.* **2018**, *4*, 37.
- (55) Musil, F.; De, S.; Yang, J.; Campbell, J. E.; Day, G. M.; Ceriotti, M. Machine learning for the structure–energy–property landscapes of molecular crystals. *Chem. Sci.* **2018**, *9*, 1289–1300.
- (56) Hansen, K.; Biegler, F.; Ramakrishnan, R.; Pronobis, W.; von Lilienfeld, O. A.; Müller, K.-R.; Tkatchenko, A. Machine Learning Predictions of Molecular Properties:



- Accurate Many-Body Potentials and Nonlocality in Chemical Space. *J. Phys. Chem. Lett.* **2015**, *6*, 2326–2331.
- (57) Xie, T.; Grossman, J. C. Crystal graph convolutional neural networks for an accurate and interpretable prediction of material properties. *Phys. Rev. Lett.* **2018**, *120*, 145301.
- (58) Pilania, G.; Wang, C.; Jiang, X.; Rajasekaran, S.; Ramprasad, R. Accelerating materials property predictions using machine learning. *Sci. Rep* **2013**, *3*, 2810.
- (59) Montavon, G.; Rupp, M.; Gobre, V.; Vazquez-Mayagoitia, A.; Hansen, K.; Tkatchenko, A.; Müller, K.-R.; Von Lilienfeld, O. A. Machine learning of molecular electronic properties in chemical compound space. *New J. Phys* **2013**, *15*, 095003.
- (60) Rupp, M.; Ramakrishnan, R.; von Lilienfeld, O. A. Machine learning for quantum mechanical properties of atoms in molecules. *J. Phys. Chem. Lett.* **2015**, *6*, 3309–3313.
- (61) Chandrasekaran, A.; Kamal, D.; Batra, R.; Kim, C.; Chen, L.; Ramprasad, R. Solving the electronic structure problem with machine learning. *npj Comput. Mater.* **2019**, *5*, 22.
- (62) Hansen, K.; Montavon, G.; Biegler, F.; Fazli, S.; Rupp, M.; Scheffler, M.; von Lilienfeld, O. A.; Tkatchenko, A.; Müller, K.-R. Assessment and Validation of Machine Learning Methods for Predicting Molecular Atomization Energies. *J. Chem. Theory Comput.* **2013**, *9*, 3404–3419.
- (63) Ma, X.; Li, Z.; Achenie, L. E.; Xin, H. Machine-learning-augmented chemisorption model for CO<sub>2</sub> electroreduction catalyst screening. *J. Phys. Chem. Lett.* **2015**, *6*, 3528–3533.
- (64) Li, Z.; Wang, S.; Chin, W. S.; Achenie, L. E.; Xin, H. High-throughput screening of bimetallic catalysts enabled by machine learning. *J. Mater. Chem. A* **2017**, *5*, 24131–24138.

- (65) Li, Z.; Ma, X.; Xin, H. Feature engineering of machine-learning chemisorption models for catalyst design. *Catal. Today* **2017**, *280*, 232–238.
- (66) Andriotis, A. N.; Mpourmpakis, G.; Broderick, S.; Rajan, K.; Datta, S.; Sunkara, M.; Menon, M. Informatics guided discovery of surface structure-chemistry relationships in catalytic nanoparticles. *J. Chem. Phys.* **2014**, *140*, 094705.
- (67) Li, H.; Zhang, Z.; Liu, Z. Application of artificial neural networks for catalysis: A review. *Catalysts* **2017**, *7*, 306.
- (68) Jinnouchi, R.; Asahi, R. Predicting Catalytic Activity of Nanoparticles by a DFT-Aided Machine-Learning Algorithm. *J. Phys. Chem. Lett.* **2017**, *8*, 4279–4283.
- (69) Gasper, R.; Shi, H.; Ramasubramanian, A. Adsorption of CO on low-energy, low-symmetry Pt nanoparticles: Energy decomposition analysis and prediction via machine-learning models. *J. Phys. Chem. C* **2017**, *121*, 5612–5619.
- (70) Kitchin, J. R. Machine learning in catalysis. *Nat. Catal.* **2018**, *1*, 230.
- (71) Neal, C. M.; Starace, A. K.; Jarrold, M. F.; Joshi, K.; Krishnamurty, S.; Kanhere, D. G. Melting of Aluminum Cluster Cations with 31–48 Atoms: Experiment and Theory. *The Journal of Physical Chemistry C* **2007**, *111*, 17788–17794.
- (72) Starace, A. K.; Neal, C. M.; Cao, B.; Jarrold, M. F.; Aguado, A.; López, J. M. Correlation between the latent heats and cohesive energies of metal clusters. *J. Chem. Phys.* **2008**, *129*, 144702.
- (73) Aguado, A.; López, J. M. Structures and stabilities of  $Al_n^+$ ,  $Al_n$ , and  $Al_n^-$  ( $n = 13–34$ ) clusters. *J. Chem. Phys.* **2009**, *130*, 064704.
- (74) Susan, A.; Joshi, K. Rationalizing the role of structural motif and underlying electronic structure in the finite temperature behavior of atomic clusters. *J. Chem. Phys.* **2014**, *140*, 154307.

- (75) Blöchl, P. E. Projector augmented-wave method. *Phys. Rev. B* **1994**, *50*, 17953–17979.
- (76) Kresse, G.; Joubert, D. From ultrasoft pseudopotentials to the projector augmented-wave method. *Phys. Rev. B* **1999**, *59*, 1758–1775.
- (77) Perdew, J. P.; Burke, K.; Ernzerhof, M. Generalized Gradient Approximation Made Simple. *Phys. Rev. Lett.* **1996**, *77*, 3865–3868.
- (78) Perdew, J. P.; Burke, K.; Ernzerhof, M. Generalized Gradient Approximation Made Simple [Phys. Rev. Lett. 77, 3865 (1996)]. *Phys. Rev. Lett.* **1997**, *78*, 1396–1396.
- (79) Kresse, G.; Hafner, J. *Ab initio* molecular-dynamics simulation of the liquid-metal–amorphous-semiconductor transition in germanium. *Phys. Rev. B* **1994**, *49*, 14251–14269.
- (80) Kresse, G.; Furthmüller, J. Efficient iterative schemes for *ab initio* total-energy calculations using a plane-wave basis set. *Phys. Rev. B* **1996**, *54*, 11169–11186.
- (81) Kresse, G.; Furthmüller, J. Efficiency of ab-initio total energy calculations for metals and semiconductors using a plane-wave basis set. *Comput. Mater. Sci.* **1996**, *6*, 15 – 50.
- (82) Pedregosa, F.; Varoquaux, G.; Gramfort, A.; Michel, V.; Thirion, B.; Grisel, O.; Blondel, M.; Prettenhofer, P.; Weiss, R.; Dubourg, V. et al. Scikit-learn: Machine Learning in Python. *J. Mach. Learn. Res.* **2011**, *12*, 2825–2830.